ARTICLES
PUBLISHED ONLINE: 1 MAY 2011 | DOI: 10.1038/NMAT3013
nature materials

High-performance flat-panel solar thermoelectric generators with high thermal concentration

Daniel Kraemer[1†], Bed Poudel[2†], Hsien-Ping Feng[1], J. Christopher Caylor[2], Bo Yu[3], Xiao Yan[3], Yi Ma[3], Xiaowei Wang[3], Dezhi Wang[3], Andrew Muto[1], Kenneth McEnaney[1], Matteo Chiesa[1,4], Zhifeng Ren[3]* and Gang Chen[1]*

The conversion of sunlight into electricity has been dominated by photovoltaic and solar thermal power generation. Photovoltaic cells are deployed widely, mostly as flat panels, whereas solar thermal electricity generation relying on optical concentrators and mechanical heat engines is only seen in large-scale power plants. Here we demonstrate a promising flat-panel solar thermal to electric power conversion technology based on the Seebeck effect and high thermal concentration, thus enabling wider applications. The developed solar thermoelectric generators (STEGs) achieved a peak efficiency of 4.6% under AM1.5G (1 kW m^{-2}) conditions. The efficiency is 7–8 times higher than the previously reported best value for a flat-panel STEG, and is enabled by the use of high-performance nanostructured thermoelectric materials and spectrally-selective solar absorbers in an innovative design that exploits high thermal concentration in an evacuated environment. Our work opens up a promising new approach which has the potential to achieve cost-effective conversion of solar energy into electricity.

At present, the two main methods of capturing solar energy for human benefit are solar photovoltaic and solar thermal processes[1–5]. Photovoltaic cells, which generate electricity by exciting electron–hole pairs, can be used as flat panels on houses, buildings and in solar farms. Solar thermal processes, on the other hand, are used in two distinct ways: electricity generation by mechanical heat engines in large power plants, and household heat supply by means of solar hot-water systems. Here, we report on a flat-panel solid-state solar thermal to electric power conversion technology for a wide range of applications that makes use of the thermoelectric effect. The efficiency of ideal thermoelectric devices (η_{te}) is determined by their operating temperature and the materials' dimensionless figure of merit (ZT), defined as $ZT = (S^2\sigma/k)T$, where S, σ, k and T are the Seebeck coefficient, electrical conductivity, thermal conductivity and absolute temperature, respectively[6,7]. The efficiency can be expressed as

$$\eta_{te} = \frac{T_h - T_c}{T_h} \frac{\sqrt{1+(ZT)_M} - 1}{\sqrt{1+(ZT)_M} + \frac{T_c}{T_h}} \quad (1)$$

where T_c is the cold-side temperature, T_h the hot-side temperature, and $(ZT)_M$ the effective ZT of the thermoelectric material between T_c and T_h. According to equation (1), an efficiency of approximately 8.6% can be reached by imposing a temperature difference of 200 °C across an ideal thermoelectric device with $(ZT)_M = 1$ and $T_c = 20$ °C. In recent years, significant progress has been made on improving thermoelectric materials[8–20], however the application of thermoelectrics in large-scale renewable energy conversion has not been demonstrated[21]. Conventional wisdom is that thermoelectrics are most suitable for waste heat recovery and that materials with significantly higher ZT are needed for large-scale applications[7,22,23]. We will show that thermoelectrics are an attractive alternative for converting solar energy into electricity.

A key challenge in solar thermoelectric power conversion is to create a significant temperature difference across the thermoelectric device with only a low solar radiation flux. Considering heat conduction only, the temperature drop across a thermoelectric element with a length L is given by $\Delta T = qL/k$, where q is the heat flux passing through the thermoelectric element and k its thermal conductivity. Taking the solar flux as 1 kW m^{-2}, corresponding to AM1.5G conditions, $L = 1$–5 mm and $k = 1$ W m^{-1} K^{-1}, the temperature drop across the thermoelectric element is only 1–5 °C, a value too small for efficient power conversion.

One approach to create a larger temperature difference is to optically concentrate the solar radiation on the thermoelectric generator to increase the heat flux. Depending on the length of the thermoelectric element, an optical concentration, C_{opt}, of 40–200 is needed to create an appreciable temperature difference of 200 °C. In 1954, Telkes[24] used a ×50 optical concentration by means of a lens to achieve a temperature difference of 247 °C across thermoelectric elements made of a p-type ZnSb alloy and an n-type Bi-based alloy, and reported an efficiency of 3.35%. However, optical concentration by a factor 40–200 requires tracking, incurring an additional cost to the system, which is unattractive, given the low efficiency.

Another approach to create the necessary temperature difference across the thermoelectric device is by using thermal concentration in a flat-panel absorber configuration, as shown in Fig. 1. A highly solar-absorbing surface (solar absorber) converts the solar radiation into heat and thermally concentrates it onto the thermoelectric elements by means of lateral heat conduction within the highly thermally conductive absorber substrate (Supplementary Information). This method of concentrating heat by conduction has been used in various solar thermal systems[4,24,25]. As illustrated in Fig. 1e, we define the thermal concentration, C_{th}, as the area

[1]Mechanical Engineering Department, Massachusetts Institute of Technology, Cambridge, Massachusetts 02139, USA, [2]GMZ Energy, 11 Wall St., Waltham, Massachusetts 02458, USA, [3]Department of Physics, Boston College, Chestnut Hill, Massachusetts 02467, USA, [4]Masdar Institute of Science and Technology, PO Box 54224, Abu Dhabi, United Arab Emirates. †These authors contributed equally to this work. *e-mail: renzh@bc.edu; gchen2@mit.edu.

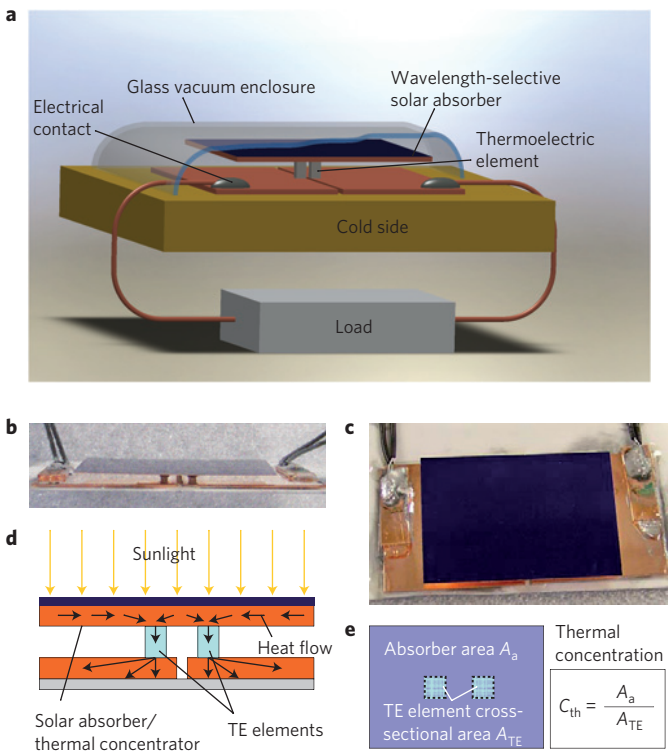

Figure 1 | Structure of a STEG cell. a, Illustration of a STEG cell made of a pair of p- and n-type thermoelectric elements, a flat-panel selective absorber that also acts as a thermal concentrator, and two bottom electrodes that serve as heat spreaders and radiation shields. The device is surrounded by a glass enclosure maintaining an evacuated environment. **b** and **c** are photographs of the device showing side (**b**) and top (**c**) views. Illustration of thermal concentration (**d**) and area ratio of absorber and cross-section of thermoelectric elements (**e**) leading to the calculation of thermal concentration.

of the absorber, A_a, divided by the cross-sectional area of the thermoelectric elements, A_{TE}. Similar to optical concentration, thermal concentration has losses, as will be discussed later. The energy flux concentration can be found by multiplying the thermal concentration and optical concentration by the opto-thermal efficiency, η_{ot}, as will be discussed later. Telkes[24] investigated a flat-panel collector STEG configuration using a black painted absorber. The highest efficiency of 0.63% was achieved with a p-type ZnSb alloy and an n-type Bi-based alloy operating in air under a temperature difference of 70 °C. Other subsequent experimental efforts, including both flat-panel STEGs for terrestrial[26] and space applications[27], and optically concentrated STEGs (refs 28–30), did not lead to better results than that reported by Telkes, despite using different materials and reaching higher temperatures. Several modelling and experimental studies have suggested that STEGs could be attractive for deep-space probe missions in near-sun orbits[31–33] because of their resistance to high radiation intensity. The terrestrial application potential of STEGs has been poor because of the low reported system efficiency, combined with the complexity and high cost of optical tracking systems for STEGs with optical concentration. In this paper we will demonstrate flat-panel STEGs with an efficiency of 4.6–5.2%, which is 7–8 times that of the best-reported value by Telkes[24]. Such flat-panel STEGs do not require tracking and can be a cost effective technology to convert solar energy into electricity.

The efficiency (η) of a STEG can be expressed as the product of the thermoelectric device efficiency (η_{te}) and the opto-thermal efficiency (η_{ot}), which is the efficiency of converting the solar radiation flux into a heat flux through the thermoelectric device

$$\eta = \eta_{ot}\eta_{te} \tag{2}$$

In Telkes' devices[24], most of the heat loss is through air convection, leading to a low opto-thermal efficiency. This heat loss can be eliminated by enclosing the device inside a vacuum. In fact, evacuated tubes are widely used in solar hot-water systems, and these tubes can routinely reach up to 200 °C without any optical concentration[34]. In China alone, there are more than 100 million m^2 of evacuated tubes deployed, generating ~73 GW of thermal power for households[35]. For an evacuated environment, the opto-thermal efficiency can be approximately expressed as (Supplementary Information)

$$\eta_{ot} \approx \tau\alpha - \frac{\varepsilon\sigma_{sb}(T_h^4 - T_{amb}^4)}{C_{opt}q_i} = \tau\alpha\left[1 - \frac{\varepsilon\sigma_{sb}(T_h^4 - T_{amb}^4)}{\tau\alpha C_{opt}q_i}\right] = \eta_{opt}\eta_{th} \tag{3}$$

where τ is the transmittance of the glass, α the absorptance and ε the effective emittance of the solar absorber, σ_{sb} the Stefan–Boltzmann constant, C_{opt} the optical concentration, T_{amb} the temperature of the surroundings and q_i the incident solar flux. The opto-thermal efficiency can be further split into the product of an optical efficiency $\eta_{opt} = \tau\alpha$ and a thermal efficiency η_{th} given by the term in the square bracket of the above equation. The above expression shows that opto-thermal efficiency decreases whereas the thermoelectric device efficiency (equation (1)) increases with increasing T_h, suggesting an optimal T_h for given τ, α, C_{opt} and q_i (Supplementary Information). When no optical concentration is used ($C_{opt} = 1$), we found that, depending on the properties of the thermoelectric material and the solar absorber, the optimal T_h is in the range of 160–250 °C, which is where Bi_2Te_3-based materials work the best. The suitability of Bi_2Te_3-based materials is expedient given the progress made in this material system in recent years[12,18,19,36–38]. Taking typical values ($\tau = 0.94$, $\alpha = 0.95$, $\varepsilon = 0.05$, $q_i = 1\,\mathrm{kW\,m^{-2}}$), it can be seen that the opto-thermal efficiency is in the range of 70–80% for a system without optical concentration operating with an absorber temperature of 200 °C. This opto-thermal efficiency, multiplied by the thermoelectric device efficiency of approximately 8%, indicates that STEGs with an efficiency of 5–6% may be achievable without any optical concentration, and even higher values are possible if a low optical concentration that does not require tracking is used. In this paper we demonstrate such a STEG with a flat-panel absorber. Our experimental results are in good agreement with the models (Supplementary Information). The high efficiency of the flat-panel STEG is achieved by the use of (1) nanostructured thermoelectric materials[12,39,40], (2) high-performance wavelength-selective solar absorbers and (3) an innovative design that uses a high thermal concentration in an evacuated enclosure that prevents air convection and conduction losses.

Our experimental devices, as illustrated in Fig. 1a–c, consist of a pair of n/p-type thermoelectric materials based on nanostructured Bi_2Te_3 alloys with their properties given in previous publications[12,39,40]. The thermoelectric elements are electrically connected in series and sandwiched between the solar absorber plate and a heat sink. The dimensions of a typical p-type thermoelectric element are $1.35 \times 1.35 \times 1.65\,\mathrm{mm^3}$ (with an uncertainty of ± 0.01 mm), and the n-type elements are of similar dimensions. Each thermoelectric element is soldered onto an individual copper plate, which represents the cold side for the thermoelectric element. The copper substrate of the solar absorber serves as a heat concentrator by conducting heat laterally to the thermoelectric elements (Fig. 1d), whereas the bottom copper plates serve as electrodes, heat spreaders, and radiation shields that reduce radiation losses from

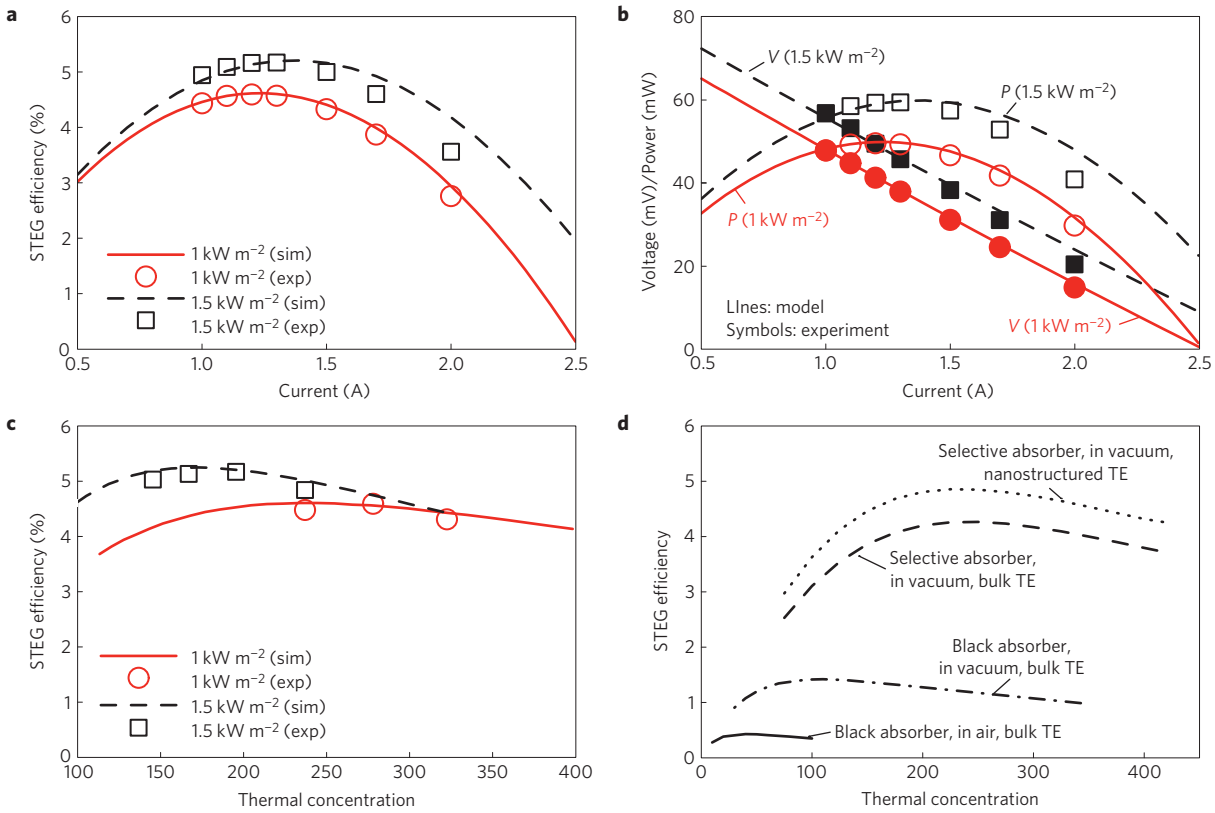

Figure 2 | STEG cell performance characteristics. Typical STEG cell characteristics at incident solar radiation fluxes of 1 kW m^{-2} and 1.5 kW m^{-2}. Open/filled squares and circles are experimental data, lines are modelling results with thermal concentrations $C_{th} = 299$ (red solid line) and $C_{th} = 196$ (black dash line). **a**, Efficiency as a function of the cell current. **b**, *I*–*V* and *I*–*P* characteristics of the STEGs. **c**, Efficiency as a function of the thermal concentration. For all experimental data, the cold side was maintained at 20 °C. **d**, Simulated efficiency of STEGs with different designs (neglecting electrical contact resistance): black absorber with traditional bulk thermoelectric materials in air (solid line); black absorber with traditional bulk thermoelectric materials in vacuum (dash-dotted line); wavelength-selective solar absorber with bulk TE materials in vacuum (dashed line); and wavelength-selective solar absorber with nanostructured bulk thermoelectric materials in vacuum (dotted line).

the rear side of the selective absorber. The size of the solar absorber must be optimized specifically for the properties and dimensions of the thermoelectric elements used and also for the absorber properties. The ratio between the absorber area, A_a, and the cross-sectional area of the thermoelectric elements, A_{TE}, is defined as the thermal concentration, C_{th}, (Fig. 1e). The devices are tested in a vacuum chamber. (See Methods for details of the experiment).

Figure 2a and b show the typical performance curves of STEGs under illumination intensities corresponding to AM1.5G (1 kW m^{-2}) and low optical concentration conditions (1.5 kW m^{-2}). The corresponding thermal concentrations of the STEGs used for 1 and 1.5 kW m^{-2} are 299 and 196, respectively. The peak efficiency is 4.6% at AM1.5G conditions and 5.2% with a solar intensity of 1.5 kW m^{-2} when the cold side is maintained at 20 °C (Fig. 2a). To experimentally simulate an optically concentrated solar flux of 1.5 kW m^{-2}, the power input of the solar simulator is adjusted. Figure 2b illustrates the typical *I*–*V* and *I*–*P* characteristics of the STEGs. The voltage output of a STEG comprising a p-type and an n-type leg can be expressed as

$$V = \int_{T_c}^{T_h} [S_p(T) - S_n(T)]\mathrm{d}T - I\left(\int_{T_c}^{T_h}\left[\frac{\rho_p}{A_p}\right]\frac{1}{\mathrm{d}T_p/\mathrm{d}x}\mathrm{d}T_p + \int_{T_c}^{T_h}\left[\frac{\rho_n}{A_n}\right]\frac{1}{\mathrm{d}T_n/\mathrm{d}x}\mathrm{d}T_n\right) \quad (4)$$

Equation (4) shows that if T_h, $\mathrm{d}T_p/\mathrm{d}x$ and $\mathrm{d}T_n/\mathrm{d}x$ are independent of the current, the voltage–current relation is linear. In reality, however, the hot-side temperature T_h, as well as the temperature distribution in the p-type and n-type element, depends on the current, leading to some nonlinearity in the *I*–*V* characteristics. The results presented are from experiments where the temperature of the solar absorber was not measured to avoid heat losses from a thermocouple. However, we measured the temperature during a few experiments and confirmed our theoretical predictions. The absorber temperature drops significantly with increasing current owing to the Peltier effect at the junction (Supplementary Information). In Fig. 2c, we plot the measured peak efficiency as a function of the thermal concentration. It can be seen that there is an optimal thermal concentration for a given thermoelectric element geometry and solar intensity (Supplementary Information). If the thermal concentration is too low, the opto-thermal efficiency η_{ot} is high because the solar absorber is at a lower temperature and the radiation loss is low; however, the thermoelectric device efficiency η_{te} is low because of the smaller temperature difference. If the thermal concentration is too high, the maximum temperature reached is too high and thus η_{ot} is too low. In addition, the ZT decreases with temperature after it reaches a maximum at about 100 °C. A higher incident solar flux of 1.5 kW m^{-2}, or 1.5 Suns, leads to a lower optimal thermal concentration, which consequently reduces the radiation losses from the absorber, yielding a higher opto-thermal efficiency. From the experimental results (Fig. 2c) we obtained the optimal thermal concentrations for the chosen dimensions of the elements of approximately 299 (AM1.5G, 1 kW m^{-2}) and 196 (1.5 kW m^{-2}).

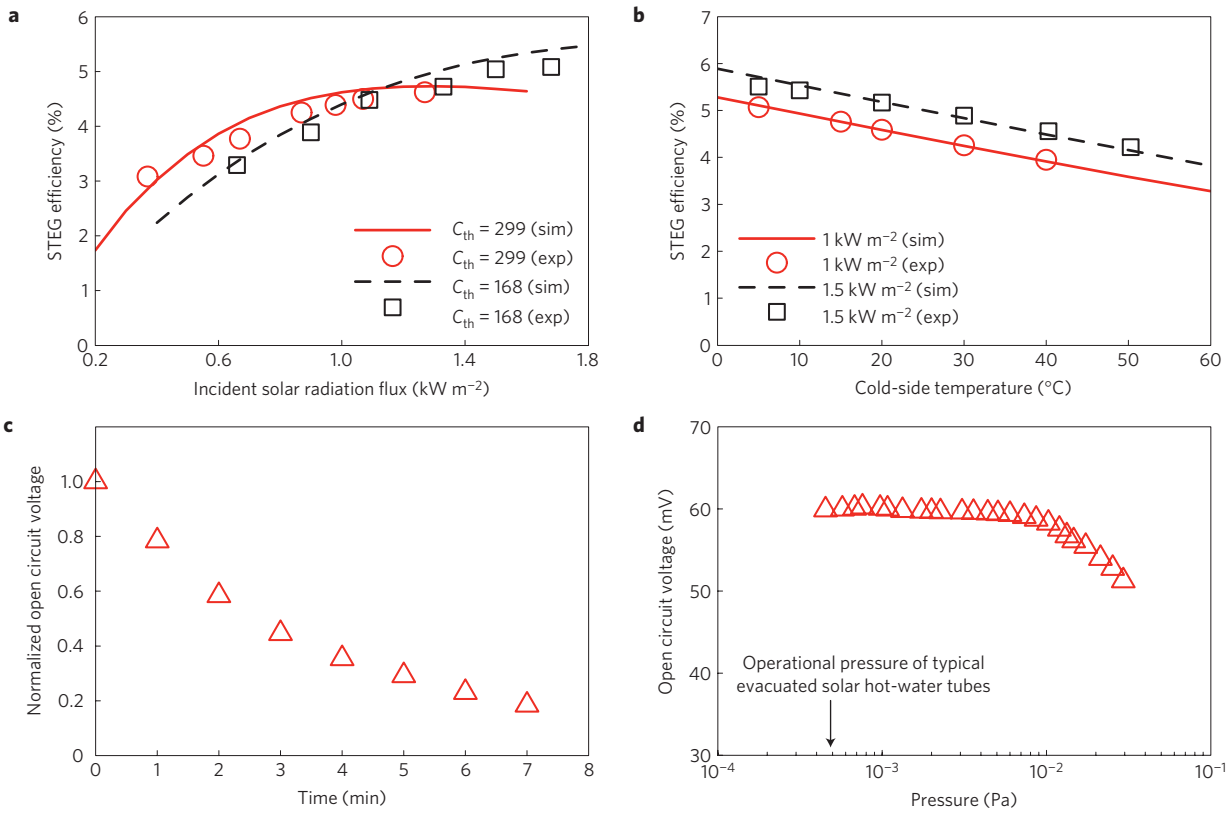

Figure 3 | Performance under varying ambient conditions. a, Efficiency dependence of STEGs on solar radiation intensity (open circles for $C_{th} = 299$ and open squares for $C_{th} = 168$). **b**, Efficiency dependence on the cold-side temperature for STEG cells optimized for 1 kW m^{-2} and 1.5 kW m^{-2}. **c**, Open circuit voltage decay as a function of time. **d**, Dependence of open circuit voltage on pressure. The arrow in **d** shows the typical operating pressure of the widely used evacuated solar collectors for hot-water systems. Symbols indicate experimental data and lines indicate modelling results.

Modelling was carried out (Supplementary Information) on the dependence of efficiency (Fig. 2a) and power output (Fig. 2b) on current, the I–V characteristics (Fig. 2b), and the dependence of efficiency on the thermal concentration (Fig. 2c) using the measured properties of the thermoelectric materials and leg dimensions. In general, the modelling results are in good agreement with the experimental results (Fig. 2a–c). The small discrepancy between modelling and experimental results can be attributed to the uncertainties in the properties used, especially the temperature dependence of the emittance of the solar absorbers. For the best fit of the experimental results, we include an electrical contact resistance that is 5% of the thermoelectric element electrical resistance. This additional electrical contact resistance results in a drop of the maximum STEG efficiency of approximately 0.2% (absolute) compared with an idealized STEG neglecting those losses, as shown in Fig. 2d.

We have tested more than 100 similar devices and routinely achieved an efficiency in the range 4.3–4.6% at AM1.5G conditions. This efficiency is seven times higher than that reported by Telkes[24]. There are several factors that enabled efficiency improvements: (1) nanostructured materials, (2) a selective surface and (3) high thermal concentration and operation in an evacuated environment. Figure 2d shows simulations carried out for different conditions to demonstrate the impact of these three factors. We have reported before on nanostructured thermoelectric materials with significantly higher ZT, especially at higher temperatures, compared to materials in the market optimized for cooling operations[12,39,40]. The effective ZT of our materials at optimal operation conditions is 1.03, whereas that of the best conventional materials is approximately 0.89. Devices built with such conventional materials will have a lower performance (dashed line in Fig. 2d). Also shown in Fig. 2d are the predicted performances of devices built with a black absorber, rather than a selective absorber, operating in both vacuum and in air (dash–dotted line and solid line). Devices operating in air can achieve a peak efficiency of ~0.5%. We also note that these three factors together not only enhance the performance of the STEG but also influence the optimal thermal concentration. Figure 2d shows that our optimized design has a much higher thermal concentration compared to STEGs operating in air with a black absorber. Consequently, our design uses less TE material and will result in cost savings.

Figure 3a shows the experimental efficiencies at different solar radiation intensities for two different thermal concentrations of 299 (open circles) and 168 (open squares), together with modelling results (solid and dashed lines). Experimental conditions were chosen such that the hot-side temperature is maintained below the solder melting point (232 °C), particularly for the experiments at higher incident radiation fluxes and higher cold-side temperatures. The experimental results show that to achieve maximum performance, STEGs should be equipped with different thermal concentrations depending on the incident solar flux. In locations with a high average solar flux the devices should have a lower average thermal concentration than devices in locations with lower avearage solar flux. For all those cases, however, the optimal operational absorber temperature of our proposed STEG design lies around 200 °C, which is significantly lower than other solar thermal power conversion technologies. In Fig. 3b, we show the dependence of the experimental efficiency on the cold-side temperature of STEGs with a thermal concentration of 299 (open circles) and 168 (open squares) together with modelling results (solid and dashed lines). The drop in efficiency is small as the temperature increases. The efficiency of the STEG

is still ~3.5%, respectively, 4% when the cold side reaches 50 °C, indicating the potential for the possible co-generation of electricity and hot water.

Another unique feature of the STEGs is the delayed thermal response resulting from the heat capacitance of the system, which enables the continuation of the power output even when the sun is partially blocked by clouds. In Fig. 3c, we show the open circuit voltage of a STEG as a function of time after the simulator is turned off. The time delay for a 50% drop in cell voltage is ~3 min. This time delay is mainly due to the heat capacitance of the solar absorber. This feature is attractive because temporary clouding can cause large power fluctuations for PV systems.

Although a vacuum is needed to eliminate air conduction heat leakage, we should point out that 106 million m^2 of evacuated solar water collectors had been installed worldwide by 2007 with a lifetime greater than 15 years[35]. As is the practice of the industry, out-gassing was compensated for by enclosing a getter in the tube to maintain a low pressure of 5×10^{-4} Pa. We show in Fig. 3d that the efficiency of our STEG changes very little when the pressure is below 10^{-2} Pa, compatible with the industrial practice used for evacuated solar hot-water collectors. The typical pressure of existing hot-water tube collectors is indicated by the arrow in Fig. 3d. Therefore, vacuum-based STEG technology is compatible with widely used evacuated solar hot-water collector tubes, indicating the potential of STEGs for co-generation of electricity and hot water, thus leading to improved system efficiency and reduced cost.

Making use of a vacuum environment in our STEG design enables the exploitation of a high thermal concentration with flat-panel absorbers. The advantages of such a high thermal concentration are that only a small amount of thermoelectric material and no complicated optical system is needed. The length of the thermoelectric elements used in our experiments are approximately 1.6 mm, which means the amount of thermoelectric bulk material used has an equivalent thickness of 5–6 μm if it were uniformly distributed over the solar absorber area. Therefore, the bulk-material-based STEGs not only have the advantage of lower manufacturing costs associated with bulk materials and devices[12] but also use smaller quantities of thermoelectric materials. For a generated electrical peak power output of 60 mW_P based on one pair of thermoelectric elements, only 0.04 g of Bi_2Te_3-based material is needed. At the current price of approximately \$250 kg^{-1} Bi_2Te_3, the cost of the thermoelectric material is about \$0.17 per electrical watt generated. Further reduction of the use of generator material is possible by using even smaller thermoelectric elements. The advantage of being able to harvest the complete solar spectrum with a small amount of thermoelectric material in a bulk form makes solar thermoelectric power conversion a promising technology.

The efficiency of STEGs can be improved by several means: (1) improving the ZT of the thermoelectric materials, (2) improving the performance of selective surfaces, especially reducing their emittance at higher temperatures, and (3) using a combination of thermal and optical concentration. Figure 4a shows the predicted maximum efficiency of a flat-panel STEG as a function of the effective ZT without optical concentration, for different effective emittance values. The optimal hot-side temperatures corresponding to the maximum efficiency are less than 250 °C, which expediently matches the working temperature range of Bi_2Te_3-based materials (the best known thermoelectric materials). Figure 4b shows the effect of varying the optical concentration while limiting the hot side to a maximum temperature of 220 °C. As can be seen from equation (2), increasing the optical concentration reduces the radiation losses and increases the opto-thermal efficiency, which leads to improved system efficiency. Results for optical concentrations less than three are particularly interesting, as such systems do not need tracking. For a fixed optical concentration and hot-side temperature, the thermal concentration

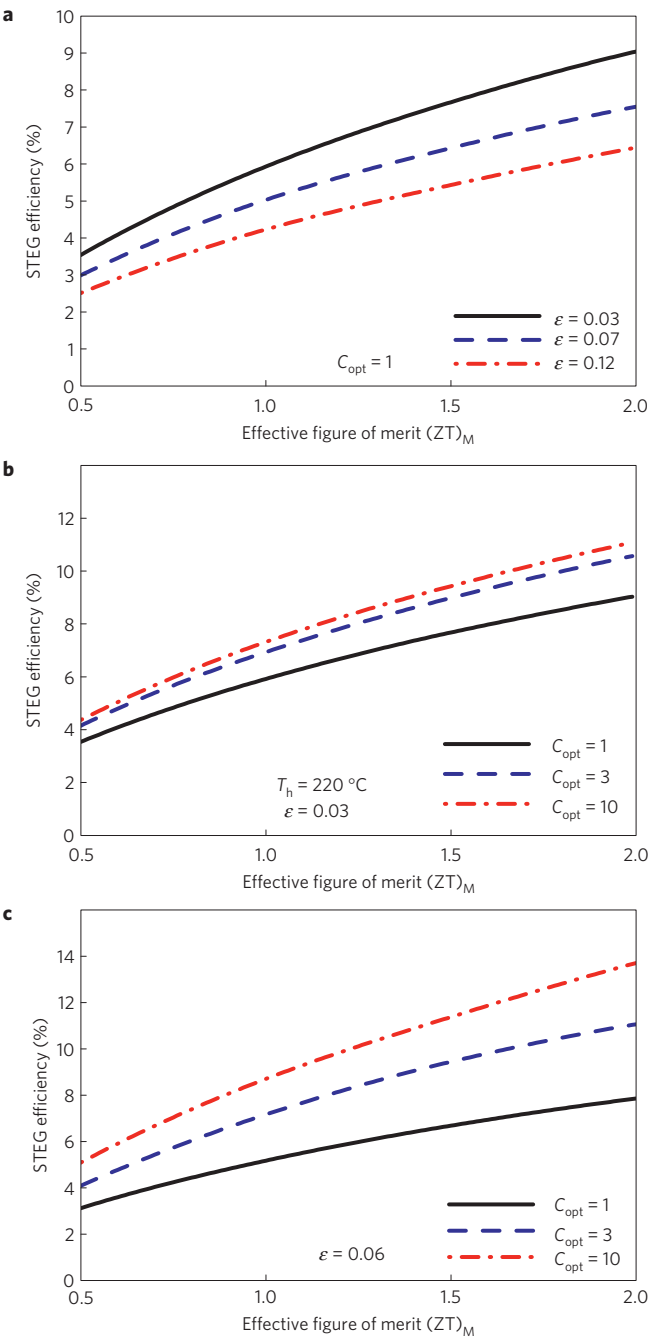

Figure 4 | Directions for improvement. Predicted STEG efficiency as a function of ZT, **a**, for different emittance values of the selective surfaces without any optical concentration, **b**, for different optical concentration ratios when the hot side is maintained at 220 °C and $\varepsilon = 0.03$, and **c**, for different optical concentration ratios with the hot-side temperature optimized by thermal concentration.

and the resulting efficiency of the STEG is determined for a specified geometry of the thermoelectric elements. Stationary STEGs with a moderate optical concentration (less than 3) can reach an efficiency of 8–10% with ZT = 1.5–2 (Fig. 4b). Figure 4c shows the maximum system efficiency as a function of ZT for different optical concentrations without a limit on the absorber temperature. For each optical concentration, the thermal concentration is optimized such that the maximum efficiency can be reached. The efficiency approaches 14% with a ZT = 2 and 10 times optical concentration (Fig. 4c) and the corresponding optimum absorber

temperature is ~300 °C for a device with similar radiative properties and geometries as those used in this paper. This temperature range of operation most likely requires multistage or segmented thermoelectric generators using different materials. Recent progress made in thermoelectric materials[8,15] raises the hope of achieving the predicted efficiency. Our experimental results demonstrate that, with further research and development, solar thermoelectric power conversion is a promising approach with the potential of becoming a key method of solar energy utilization.

Methods

To vary the cold-side temperature the copper plates are mounted onto a ceramic plate for electrical insulation and put in good thermal contact with a temperature-controlled sample holder. In practical applications, the cooling mechanism and the operational cold-side temperature will depend on the application. A passive heat sink to the environment based on natural convection will be sufficient to maintain the cold-side at a temperature similar to the operational temperature of PV cells. A commercial solar absorber is used, which is a multi-layer thin-film spectrally-selective surface on a copper substrate. The copper side of the solar absorber is in both thermal and electrical contact with the thermoelectric elements (Fig. 1). The selective surface has a specified solar absorptance of 94.4% and a thermal emittance of ~5% at 100 °C (Supplementary Information). The rear side of the solar absorber and the front side of each bottom copper plate are polished to reduce their emittance. The vacuum levels are maintained in the range of 5×10^{-4}–3×10^{-2} Pa during the experiments. In comparison, the typical vacuum level of evacuated solar hot-water tubes is 5×10^{-4} Pa (ref. 34).

The optimum design of the STEGs depends on the incident solar radiation power, the solar absorber properties, the thermoelectric material properties, the cold-side temperature, and the device geometry. Numerical simulations determine the optimum absorber plate sizes for the thermoelectric elements that are used in the experiments (Supplementary Information). The actual energy flux concentration provided to the thermoelectric elements is the product of the thermal concentration, the optical concentration, and the opto-thermal efficiency (equation (3)) at the operational temperature. The thermal flux concentration is system specific and dependent on operational conditions such as incident flux and cold-side temperature. Modelling results show that the temperature drop within the solar absorber is smaller than 2 °C for the thermal concentrations used (Supplementary Information). The temperature drop along the bottom copper plates is even smaller.

A solar simulator with an AM1.5G filter is used as the light source. The incident flux is measured with a calibrated power meter provided by the manufacturer of the solar simulator. In addition, we also use an NREL-calibrated solar cell to cross-check the radiation flux. The thermoelectric devices, similar to PV, need load optimization to maximize the power output. We determine the optimal load condition by using a current source as a variable resistor[41], and we simultaneously measure both the current and the voltage drop across the copper electrodes on the cold side. The STEG efficiency, $\eta = IV/(q_i A_a)$, is calculated from the voltage V, the current I, the absorber area A_a and the incident solar radiation flux q_i. This efficiency includes the glass transmission loss and the solar absorber loss as well as possible parasitic electrical and thermal losses of the system. The transmittance of the glass enclosure is measured to be 94%.

Received 12 July 2010; accepted 23 March 2011; published online 1 May 2011

References

1. Lewis, N. *et al. Basic Research Needs for Solar Energy Utilization*. (DOE Office of Science, 2005); available at http://www.er.doe.gov/bes/reports/abstracts.html.
2. Luque, A. & Hegedus, S. *Handbook of Phovoltaic Science and Engineering* (Wiley, 2003).
3. Green, M. A. *Third Generation Photovoltaics: Advanced Solar Energy Conversion* (Springer, 2003).
4. Mills, D. Advances in solar thermal electricity technology. *Sol. Energy* **76,** 19–31 (2004).
5. Roeb, M. & Muller-Steinhagen, H. Concentrating on solar electricity and fuels. *Science* **329,** 773–774 (2010).
6. Goldsmid, H. J. *Thermoelectric Refrigeration* (Plenum, 1964).
7. Rowe, D. M. *Thermoelectrics Handbook Nano to Macro* (CRC Taylor & Francis, 2006).
8. Venkatasubramanian, R., Siivola, E., Colpitts, T. & O'Quinn, B. Thin-film thermoelectric devices with high room-temperature figures of merit. *Nature* **413,** 597–602 (2001).
9. Harman, T. C., Taylor, P. J., Walsh, M. P. & LaForge, B. E. Quantum dot superlattice thermoelectric materials and devices. *Science* **297,** 2229–2232 (2002).
10. Hsu, K. F. *et al.* Cubic $AgPb_mSbTe_{2+m}$: Bulk thermoelectric materials with high figure of merit. *Science* **303,** 818–821 (2004).
11. Dresselhaus, M. S. *et al.* New directions for low-dimensional thermoelectric materials. *Adv. Mater.* **19,** 1043–1053 (2007).
12. Poudel, B. *et al.* High-thermoelectric performance of nanostructured bismuth antimony telluride bulk alloys. *Science* **320,** 634–638 (2008).
13. Heremans, J. P. *et al.* Enhancement of thermoelectric efficiency in PbTe by distortion of the electronic density of states. *Science* **321,** 554–557 (2008).
14. Boukai, A. I. *et al.* Silicon nanowires as efficient thermoelectric materials. *Nature* **451,** 168–171 (2008).
15. Hochbaum, A. I. *et al.* Enhanced thermoelectric performance of rough silicon nanowires. *Nature* **451,** 163–167 (2008).
16. Snyder, G. J. & Toberer, E. S. Complex thermoelectric materials. *Nature Mater.* **7,** 105–114 (2008).
17. Rhyee, J-S. *et al.* Peierls distortion as a route to high thermoelectric performance in In_4Se_3-delta crystals. *Nature* **459,** 965–968 (2009).
18. Zhao, X. B. *et al.* Bismuth telluride nanotubes and the effects on the thermoelectric properties of nanotube-containing nanocomposites. *Appl. Phys. Lett.* **86,** 062111 (2005).
19. Tang, X. F. *et al.* Preparation and thermoelectric transport properties of high-performance p-type Bi_2Te_3 with layered nanostructure. *Appl. Phys. Lett.* **90,** 012102 (2007).
20. Tritt, T. M. & Subramanian, M. A. (eds) Energy harvesting through thermoelectrics: Power generation and cooling. *MRS Bull.* **31,** 188–194 (2006).
21. Vining, C. B. An inconvenient truth about thermoelectrics. *Nature Mater.* **8,** 83–85 (2009).
22. Yang, J. H. & Stabler, F. R. Automotive applications of thermoelectric materials. *J. Electron. Mater.* **38,** 1245–1251 (2009).
23. Bell, L. Cooling, heating, generating power, and recovering waste heat with thermoelectric systems. *Science* **321,** 1457–1461 (2008).
24. Telkes, M. Solar thermoelectric generators. *J. Appl. Phys.* **25,** 765–777 (1954).
25. Tobias, I. & Luque, A. Ideal efficiency and potential of solar thermophotonic converters under optically and thermally concentrated power flux. *IEEE Trans. Electron Devices* **49,** 2024–2030 (2002).
26. Goldsmid, H. J., Giutronich, J. E. & Kaila, M. M. Solar thermoelectric generation using bismuth telluride alloys. *Sol. Energy* **24,** 435–440 (1980).
27. Rush, R. *Solar Flat Plate Thermoelectric Generator Research*. Tech. Doc. Rep. Air Force AD 605931 (General Electric Corp., 1964).
28. Dent, C. L. & Cobble, M. H. *Proc. 4th Int. Conf. on Thermoelectric Energy Conversion* 75–78 (IEEE, 1982).
29. Mgbemene, C. A., Duffy, J., Sun, H. & Onyegegbu, S. O. *ASME Conf. Proc. ES2008* (ASME, 2008).
30. Li, P. *et al.* Design of a concentration solar thermoelectric generator. *J. Electron. Mater.* **39,** 1522–1530 (2010).
31. Fuschillo, N. & Gibson, R. Germanium-silicon, lead telluride, and bismuth telluride alloy solar thermoelectric generators for venus and mercury probes. *Adv. Energy Conversion* **7,** 43–52 (1967).
32. Raag, V., Berlin, R. E., Bifano, & Bifano, W. J. *Intersociety Energy Conversion Engineering Conf.* (1968).
33. Scherrer, H., Vikhor, L., Lenior, B., Dauscher, A. & Poinas, P. Solar thermolectric generator based on skutterudites. *J. Power Source* **115,** 141–148 (2003).
34. Yin, Z. Q. Development of solar thermal systems in China. *Sol. Energy Mater. Sol. Cells* **86,** 427–442 (2005).
35. Weiss, W., Bergmann, I. & Stelzer, R. *Solar Heat Worldwide, Markets and Contribution to the Energy Supply 2007* (International Energy Agency, 2009).
36. Wang, S., Xie, W., Li, H. & Tang, X. High performance n-type $(Bi,Sb)_2(Te,Se)_3$ for low temperature thermoelectric generator. *J. Phys. D* **43,** 335404 (2010).
37. Xie, W., Tang, X., Yan, Y., Zhang, Q. & Tritt, T. M. High thermoelectric performance BiSbTe alloy with unique low-dimensional structure. *J. Appl. Phys.* **105,** 113713 (2009).
38. Bulat, L. P. *et al.* Bulk nanostructured polycrystalline p–Bi–Sb–Te thermoelectrics obtained by mechanical activation method with hot pressing. *J. Electron. Mater.* **39,** 1650–1653 (2010).
39. Ma, Y. *et al.* Enhanced thermoelectric figure-of-merit in p-type nanostructured bismuth antimony tellurium alloys made from elemental chunks. *Nano Lett.* **8,** 2580–2584 (2008).
40. Yan, X. *et al.* Experimental studies on anisotropic thermoelectric properties and structures of n-type $Bi_2Te_{2.7}Se_{0.3}$. *Nano Lett.* **10,** 3373–3378 (2010).
41. Muto, A., Kraemer, D., Hao, Q., Ren, Z. F. & Chen, G. Thermoelectric properties and efficiency measurements under large temperature differences. *Rev. Sci. Instrum.* **80,** 093901 (2009).

Acknowledgements

This material is partially based on work supported as part of the 'Solid State Solar-Thermal Energy Conversion Center (S^3TEC)', an Energy Frontier Research Center funded by the

US Department of Energy, Office of Science, Office of Basic Energy Sciences under Award Number: DE-SC0001299/DE-FG02-09ER46577 (G.C. and Z.F.R.) and MIT-Masdar program (G.C. and M.C.).

Author contributions

D.K. carried out modelling and simulation, initial STEG-efficiency experiments, and contributed to the manuscript preparation; B.P. conducted the experiments reported in the paper; H-P.F., J.C.C. and B.Y. contributed to the development of electrical contacts used for devices; X.Y. made the n-type TE elements; Y.M. fabricated the devices; X.W. prepared the absorbers; D.W. assisted in making the TE elements and electrical contacts; A.M. performed device testing; K.M. participated in device modelling and manuscript preparation; M.C. contributed to research planning and student (D.K.) supervision; Z.F.R. directed materials and device research at BC, and contributed to manuscript preparation; G.C. originated the idea and contributed to the manuscript preparation, in addition to directing research at MIT.

Additional information

The authors declare competing financial interests: details accompany the paper at www.nature.com/naturematerials. Supplementary information accompanies this paper on www.nature.com/naturematerials. Reprints and permissions information is available online at http://www.nature.com/reprints. Correspondence and requests for materials should be addressed to Z.F.R. or G.C.